A Workflow for Building Surface-Based Reservoir Models Using NURBS Curves, Coons Patches, Unstructured Tetrahedral Meshes and Open-Source Libraries

Zhao Zhang*

Institute of Petroleum Engineering, Heriot-Watt University, Edinburgh, EH14 4AS, UK

Zhen Yin

Department of Geological Sciences, Stanford University, CA, 94305

Xia Yan

School of Petroleum Engineering, China University of Petroleum (East China), Shandong, China

Abstract

Surface-based models have been built to represent complex reservoir geometries. This paper presents a workflow for building surface-based reservoir models using NURBS curves, Coons patches and unstructured tetrahedral volume meshes. Surfaces are created as Coons patches based on NURBS curves. The surface mesh of the entire model is hybrid consisting of quadrilaterals and triangles. Geological regions are represented as volumes bounded by surfaces. Unstructured tetrahedral meshes are built to adapt to the bounding surfaces. Well configurations of location and geometry are particularly flexible, facilitated by mesh adaptation. All libraries for curve, surface and mesh generation are open-source. They are free-of-charge for non-commercial uses. The workflow provides a flexible alternative to commercial software packages for building surface-based models and unstructured meshes. The workflow is validated by simulating two-phase immiscible displacement and comparing

*Corresponding author

Email address: zhao.zhang@hw.ac.uk (Zhao Zhang)

to the analytical solution.[1]

Keywords: NURBS, Coons patch, unstructured tetrahedral mesh, surface-based reservoir modelling, open-source

1. Introduction

The conventional practice in hydrocarbon reservoir modelling is based on corner-point grids (CPG). As uncertainty is reduced in an oil or gas field with more exploration and production data becoming available, usually only a single detailed, history-matched, full-field, base-case model is maintained (Bentley, 2016). The model is then upscaled for simulation. The main disadvantages of this practice include that it is difficult and very time-consuming to change the underlying geological concepts of a detailed model; hard to explore a range of reservoir prototypes; the geometry of the geological architectures is grid dependent and CPG limit the geometric complexities that can be captured.

Another approach is to build surface-based reservoir models (SBRM) such that the model can be grid-independent (Bentley and Ringrose, 2017). Surfaces that separate the model into different volumes or regions are built in the reservoir prototyping phase (Cavero et al., 2016) and are enriched as new data become available. The idea of SBRM has been applied in software packages such as GSI3D, Move and Gocad.

Volumes bounded by the surfaces need to be meshed for simulation. In general, there are two types of meshes which are structured (e.g. Cartesian, curvilinear or corner-point grids) and unstructured meshes (e.g. unstructured tetrahedral, polyhedral or hybrid meshes). Compared to structured grids, unstructured meshes offer a more flexible way to adapt to complex geometries automatically such that meshes conform to model architectures rather than model architectures conforming to meshes (Milliotte and Matthäi, 2014; Kumar et al., 2016). This explains the popularity of unstructured meshes in computer aided engineering (CAE) or design (CAD). There are a number

[1]The contribution of Zhao Zhang is the development and implementation of the workflow and the writing of the paper. The contribution of Zhen Yin is help with the introduction of the paper and analysis of how to build NURBS curves from seismic, outcrop and sparse data. The contribution of Xia Yan is help with the design of test cases. All authors have approved the paper and agree its submission.

of commercial or free 3D unstructured mesh generators for CAE or CAD, including ANSYS Meshing, STAR-CCM+, GMSH, Gocad FEMC, Abaqus and Pointwise. A comparative study of workflows using some of these software packages for unstructured mesh generation with SBRM is reported in Zehner et al. (2015).

Question is: can we build SBRM and unstructured meshes using freely available and open-source codes? The answer is yes. In this paper, we will present a workflow of constructing SBRM and unstructured meshes based on open-source codes and libraries. A model builder written in Matlab and a mesh generator written in C++ are developed to implement the workflow. All libraries are incorporated internally for efficiency and we only need files for exporting data from the model builder to the mesh generator.

Non-uniform Rational Basis Spline (NURBS) is commonly used in the computer aided design community for describing curves and surfaces (Piegl and Tiller, 2012). It has also been applied to geological modelling (Zhong et al., 2006). Here we use NURBS for generating curves and bilinearly blended Coons patches (BBCP) for surfaces. The approach is termed NURBS-Curves-BBCP. A Coons patch is a type of manifold parametrization used in computer graphics (Farin and Hansford, 1999). We only need four curves to generate a BBCP. The functions for generating NURBS and BBCP are available in the open-source Matlab codes NURBS Toolbox.

To make reservoir models reliable, reservoir geological structures interpreted from 2D/3D seismic and outcrop observations can be used to guide the generation of curves and surfaces (Novakovic et al., 2002; Ruiu et al., 2016; Colombera et al., 2018). Besides, sparse data observations such as well data (e.g. horizon picks) can also be assimilated to the NURBS curves to further correct the reservoir models. Compared to NURBS surfaces Ruiu et al. (2016), the NURBS-Curves-BBCP approach requires less inputs (only curves) to generate 3D models. Another important advantage of the NURBS-Curves-BBCP approach is that it enables more flexible update of reservoir models when new structure patterns are discovered during the reservoir development. For example, it is found that 4D seismic monitoring acquired after the reservoir production can detect new reservoir structures which are initially not interpreted from the 3D seismic (Yin et al., 2015). It therefore requires the reservoir model structures to be updated. But the update of reservoir structural models can be complex and very time consuming if using the conventional CPG modelling. This problem is avoided in NURBS by simply updating the curves.

The connection between Coons patches and unstructured volume mesh generation is a surface mesh of the entire model. The surface mesh needs to adapt to all intersection curves between surfaces to be water-tight, which is a requirement for generating a volume mesh for simulation. However, there is no open-source codes for generating a 3D surface mesh on a given set of Coons patches.

In the current study, a hybrid surface mesh is built for the entire model. Structured logically Cartesian grids are constructed on Coons patches. Intersection curves on each vertical bounding surface are discretised into a Planar Straight Line Graph (PSLG) which is read into the open-source C library Triangle (Shewchuk, 1996, 2002) to generate adaptive triangular meshes . Then the meshes on Coons patches and vertical bounding surfaces are connected to form a surface mesh of the entire model.

The open-source C++ library TetGen (Si, 2015) is employed for unstructured volume mesh generation. The hybrid surface mesh is stored as a Piecewise Linear Complex (PLC) which is the input format for TetGen. Tetrahedral meshes adapt to bounding surfaces in the sense that the surfaces can be represented as the connected facets of tetrahedral elements. Quality mesh generation according to constraints and local refinement are available in TetGen. An alternative for TetGen could be CGALmesh which is part of the CGAL library. However as reported in Si (2015), TetGen is more computationally efficient than CGALmesh. Both TetGen and CGALmesh allows compiling them as internal libraries. As CGALmesh is dependent on other libraries in CGAL, using CGALmesh requires incorporating all these libraries which is less convenient than using TetGen.

Some other studies for unstructured mesh generation on 3D geological models can be found in literature. Wang et al. (2017) presented an approach for generating Delaunay discretisation for 3D discrete fracture networks where they generate Delaunay triangular meshes on surfaces and then use TetGen to create adaptive tetrahedral meshes. However, all surfaces in their study are flat while curved surfaces are considered in our study. Pellerin et al. (2017) developed a library for reading and writing surface and volume meshes in various formats to help researchers interact with different software packages of mesh generation, simulation and visualisation. The library can be used with our workflow to convert volume meshes generated by TetGen into formats compatible with different software packages.

This paper is organised as follows. First, open-source codes NURBS Toolbox, Triangle and TetGen are reviewed. Second, the workflow of building SBRM, hybrid surface meshes and adaptive volume meshes is discussed. Third, mesh post-processing techniques are reviewed. Finally, test cases for our workflow are presented.

2. Review of Open-Source Libraries

2.1. NURBS Toolbox

NURBS stands for Non-uniform Rational Basis Spline. It is the standard for describing and modelling curves and surfaces in CAD and computer graphics. For an introduction to the mathematical theories of NURBS, please see Rogers (2000) and Piegl and Tiller (2012). A NURBS curve is described by a list of control points and a knot vector. A curve is represented as a series of polynomials defined by the control points. The knots determine the start and end locations of the polynomials. The number of control points should be at least equal to the order of the curve, while the length of the knot vector is the sum of the number of control points and the order of the curve. Knots are defined in the parametric space. In the current study, the open-source Matlab library NURBS Toolbox is employed (Spink, 2010) for both NURBS curves and Coons patches. For a curve, the range of the values of knots is $[0, 1]$ in NURBS Toolbox. Here, we use quadratic curves.

A Coons patch is a type of manifold parametrization (Farin and Hansford, 1999). Given four boundary curves, a parametric surface can be generated as a bilinearly blended Coons patch that interpolates to the curves. The parametric definition of a surface is

$$\mathbf{x} = (x, y, z) = f(u, v) \ , \tag{1}$$

where (x, y, z) is the location in 3D, u and v are the parametric coordinates and f is a mapping function. In NURBS Toolbox, the range of u and v is [0,1] which does not contain information of the aspect ratio (length of longest side over that of shortest side) of a 3D surface. Four boundary curves are

$$f(0, v), \quad f(1, v), \quad f(u, 0), \quad f(u, 1), (0 \leq u \leq 1, 0 \leq v \leq 1). \tag{2}$$

The definition of a bilinearly blended Coons patch is (Farin and Hansford, 1999)

$$
\begin{aligned}
f(u,v) &= (1-u)f(0,v) + uf(1,v) \\
&\quad +(1-v)f(u,0) + vf(u,1) \\
&\quad -[1-u,u]\begin{bmatrix} f(0,0) & f(0,1) \\ f(1,0) & f(1,1) \end{bmatrix}\begin{bmatrix} 1-v \\ v \end{bmatrix}\ ,
\end{aligned}
\tag{3}
$$

which is the sum of two linear interpolations minus a bilinear interpolation.

2.2. Triangle

The open-source C library Triangle (Shewchuk, 1996, 2002) is adopted for Delaunay triangulation in 2D. Triangle has been applied in various areas and has been cited several thousand times (De Berg et al., 2000; Tu et al., 2018; Welsh and Mainland, 2004). It can generate exact Delaunay triangulations (DT), constrained DT, conforming DT, Voronoi diagrams, high-quality triangular meshes and refine existing triangulations (Chew, 1993). Constraints on angles and areas of triangles can be implemented for high-quality mesh generation. Both incremental and divide-and-conquer algorithms for DT are available (Guibas and Stolfi, 1985). Besides, the maximum allowed number of Steiner points can be precisely controlled during triangulation.

The input for Triangle is a Planar Straight Line Graph (PSLG) that is a collection of edges and associated vertices. The constraints for mesh generation on each surface are four boundary curves and internal intersection curves. The edges of a PSLG cannot be subdivided in a constrained DT, but may be subdivided in a conforming DT. In other words, Steiner points are allowed in a conforming DT but not a constrained DT. Yet, some triangles in a constrained DT might not be Delaunay.

2.3. TetGen

The open-source TetGen library in C++ (Si, 2015) is adopted for unstructured tetrahedral mesh generation. TetGen can be used as either a standalone program or a library component integrated in other software. It generates constrained Delaunay tetrahedralizations, boundary conforming Delaunay meshes and Voronoi partitions. Given a surface mesh, TetGen can tessellate the interior of the domain and preserve the boundary. Steiner points may be added on the boundary for mesh quality. However, a function in TetGen for enforcing that no Steiner points can be added is also available.

This is useful for joining two volume meshes sharing the same boundary surface. Various constraints and refinement options are provided in TetGen. Briefly, they include:

1. Minimum dihedral angle and maximum radius-edge ratio for the quality of tetrahedral elements.
2. Maximum volume and facet area for tetrahedral elements.
3. User-defined isotropic mesh sizing functions specifying desired edge lengths at any nodal locations. Histograms of mesh quality can be printed.
4. Adaptive remeshing with respect to newly added nodes. If no nodes are added, the mesh can be reconstructed for mesh refining or coarsening.

The input boundary representation (B-Rep) for TetGen is a Piecewise Linear Complex (PLC) (Miller et al., 1996), which is a format of storing the surface mesh for the entire 3D model. A PLC does not have to be a manifold (Lee, 2010), indicating that it can contain internal boundaries, which is needed for generating surface-based reservoir models. Each surface in a PLC is associated a unique marker, which can be passed to corresponding triangular facets in the volume mesh for assigning boundary conditions. Regions in a PLC are defined by the coordinates of a node in each region. Each region has a unique integer marker, which can be passed to corresponding elements in the volume mesh for assigning petrophysical properties.

3. Adaptive Surface and Volume Mesh Generation

The general workflow of building surface-based reservoir models with NURBS curves, Coons patches, adaptive unstructured surface and volume meshes is presented in Fig. 1. Given the open-source libraries, curves and surfaces can be built using NURBS Toolbox, while tetrahedral volume meshes can be generated by TetGen. The link between 3D surfaces and volume mesh is a surface mesh of the entire model. For each Coons patch, a structured logically Cartesian grid is built. For the four vertical bounding surfaces, unstructured triangular meshes are generated to adapt to internal curves. Then a hybrid surface mesh of the entire model consisting of quadrilaterals and triangles as elements is obtained by connecting all structured and unstructured surface meshes.

The workflow for building 3D models and mesh generation involves a model builder written in Matlab and a mesh generator in C++. The model builder is based on NURBS Toolbox; the mesh generator is based on Triangle and TetGen. Structured grids and PLSGs are built in the model builder and exported to .txt files. The files are subsequently read into the mesh generator for unstructured surface and volume mesh generation. Triangle and TetGen are compiled as internal libraries. The inputs for both Triangle and TetGen are internal. Codes of the model builder and mesh generator can be downloaded from the linked Mendeley dataset. The detailed steps of the workflow are as follows.

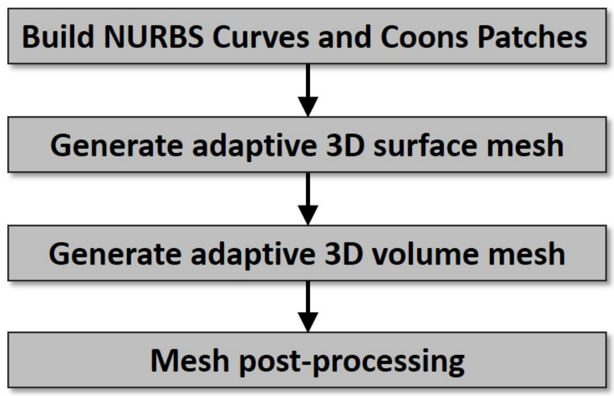

Figure 1: Workflow of building surface-based reservoir models with NURBS curves, Coons-Patches, adaptive unstructured surface and volume meshes.

1. Design a surface-based reservoir model consisting of NURBS curves and four vertical bounding surfaces (see Section 5.1).
2. Build NURBS curves and Coons patches using NURBS Toolbox. Two Coons patches are not allowed to intersect since it is computationally expensive to find the exact position of the intersection curve (Abdel-Malek and Yeh, 1996). Therefore, if two surfaces intersect, we define a new NURBS curve as the intersection curve, and then build Coons patches treating the intersection curve as one of the bounding curves. This is illustrated in Fig. 2.
3. Build a structured logically Cartesian grid on each Coons patch. Export all these structured surface grids from the model builder into a .txt file.
4. Record NURBS curves on four vertical bounding surfaces. Each vertical surface has two NURBS curves as top and bottom bounding curves,

two vertical left and right bounding lines, and other NURBS curves as internal curves. Then for each vertical surface, discretize all curves into segments. The segment length should be consistent with the structured grid on Coons patches. A PSLG of a vertical surface is obtained by assembling all segments of NURBS curves and segments on the two vertical bounding lines. Export four PSLGs of the four vertical bounding surfaces from the model builder into a .txt file.

5. Read structured surface grids and PSLGs from the .txt files into the mesh generator.
6. Triangle is called by the mesh generator to build a 2D unstructured triangular mesh for each PSLG (the data structure *triangulateio* is used to pass the PSLG into Triangle. Detailed guidance on user controls about mesh quality can be found in Shewchuk (2005)). The 2D coordinates of a PSLG are obtained straightforwardly by ignoring the constant x or y coordinate since each PSLG is on a flat vertical surface (see Appendix A for unstructured mesh generation using Triangle on a 3D curved surface). Then the constant coordinate is added accordingly after mesh generation to obtain a 3D surface mesh. If Steiner points are created on the boundary curves of one surface, they must be treated as additional constraints during mesh generation on neighbouring surfaces such that the discretisation of a curve stays the same on neighbouring surfaces. Therefore, Steiner points are prohibited in the current study to avoid extra computational complexity.
7. Connect structured grids on Coons patches and unstructured meshes on vertical bounding surfaces to obtain a surface mesh in PLC format of the entire model. Then TetGen is called by the mesh generator to build a tetrahedral mesh based on the PLC (the data structure *tetgenio* is used to pass the PLC into TetGen. Detailed guidance on user controls about mesh quality can be found in Si (2013)). Repeating nodes on curves shared between neighbouring surfaces could be retained as TetGen would neglect them automatically. However, self-intersections (e.g. an endnode of an edge lies in the interior of a triangle) are not allowed and can be detected by TetGen.

4. Mesh Post-Processing

The basic data structures of an unstructured tetrahedral mesh include a list of nodes' coordinates and a list of elements' connectivity. The purpose

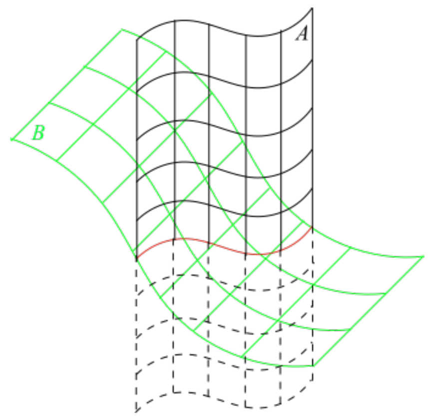

Figure 2: If two surfaces A and B intersect, a new red NURBS curve is defined. Then both A and B are generated as two Coons patches each.

of mesh post-processing is to generate further information in preparation for flow computations. Node-centred finite or control volume methods are widely used for discretisation. An edge-based data structure can be employed to facilitate the implementation of control volume discretisation for partial differential equations (PDE) and reduce computational and storage costs (Lyra et al., 2004; Zhao and Zhang, 2000; Sun et al., 2010; Al Qubeissi, 2013; Akkurt and Sahin, 2017). Mesh post-processing for the edge-based data structure has been implemented in Zhang (2015) and is reviewed here. The post-processing steps mainly include the construction of the following data structures in sequence (Löhner, 2008):

- Elements surrounding nodes: An element surrounds a node if the node is one of the four vertices of the element. The number of elements surrounding each node varies in an unstructured mesh.

- Nodes surrounding nodes: this data structure is built based on elements surrounding nodes. If node i is one of the vertices of elements surrounding node j, then the two nodes are neighbours. The number of nodes surrounding each node varies in an unstructured mesh.

- Edges surrounding nodes: Edges are only built between neighbouring nodes. For each edge, the shared faces between the corresponding control volumes of the two endnodes are computed. The edges-surrounding-nodes structure can simplify the discretisation scheme for unstructured meshes and reduce computational cost.

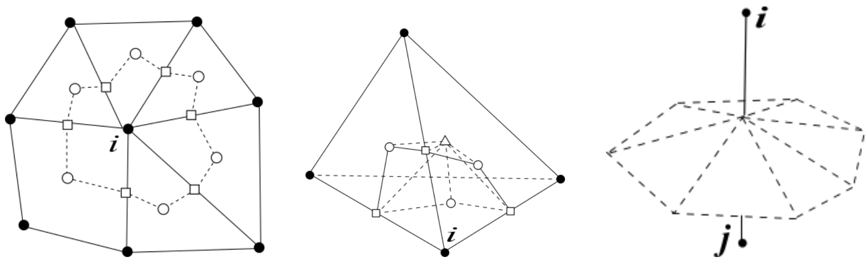

(a) Control volume construction in 2D (b) Control volume construction in 3D (c) Edge-based data structure

Figure 3: Solid nodes belong to the primary finite element mesh, small circles are centroids of polygons, small squares are edge midpoints, and small triangles represent tetrahedron centroids.

- Build edge-based data structure by grouping shared faces between two control volumes to facilitate discretisation. The implementation is non-trivial and details using pseudocodes can be found in Appendix B.

Figs. 3a and 3b show the control volume construction in 2D and 3D, respectively. In 2D, a segment of the control volume boundary is built between the centroid of a polygon and the midpoint of an edge. Each polygon surrounding node i contains two segments. The control volume of node i is built by connecting all these segments. In a 3D tetrahedral mesh, each tetrahedron surrounding node i contributes six triangular bounding faces for the control volume. The figure shows one of the tetrahedrons. Each triangular bounding face is formed by connecting the centroid of the tetrahedron, a face centroid and an edge midpoint. The control volume of node i in 3D is built by connecting all these bounding faces. The shared faces of control volumes around nodes i and j are grouped to form a small umbrella shown in Fig.3c which is an edge-based data structure.

5. Test Cases

5.1. 3D Model and Volume Mesh Generation

The conceptual geological model is bounded by Coons patches and the four vertical bounding surfaces. Fig. 4 shows the NURBS curves for building Coons patches. These curves represent the intersection between surfaces and cross-sections. Fig. 5 shows the Coons patches built from the curves, where colours correspond to heights (z-coordinates). The Coons patches are represented as structured logically Cartesian grids. Fig. 6 shows the surface mesh of the entire model. The surface mesh is hybrid and consists of quadrilaterals and triangles as elements. Unstructured triangular meshes are built on the four vertical bounding surfaces to adapt to internal intersection curves.

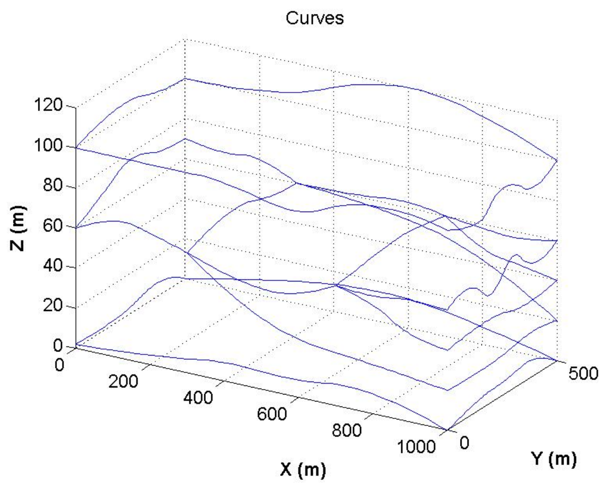

Figure 4: NURBS curves for a geological model. The curves represent the intersection between surfaces and cross-sections.

TetGen allows remeshing with respect to newly added nodes. Therefore, we represent wells as discrete nodes with marks corresponding to wells. The marks are used to identify nodes at wells after remeshing. In addition, triangular facets on boundaries are identified by associated boundary marks.

Fig. 7 shows an unstructured tetrahedral volume mesh built from the parametric surfaces in Fig. 5. It contains 12610 nodes and 70879 tetrahedral elements. All bounding surfaces and curves are precisely respected. Geological regions bounded by surfaces are identified using TetGen by the coordinates of a node inside each region. Taking the four vertical surfaces into account, the 3D model consists of eleven surfaces bounding four regions. As a validation example of mesh generation, homogeneous properties are assigned to each region. The colours in Fig. 7 correspond to horizontal permeability values. It is usually more robust to generate low-quality volume mesh (e.g. without constraints on minimum dihedral angle or maximum edge-radius ratio) first, and then refine the mesh to increase quality and adapt to nodes at wells.

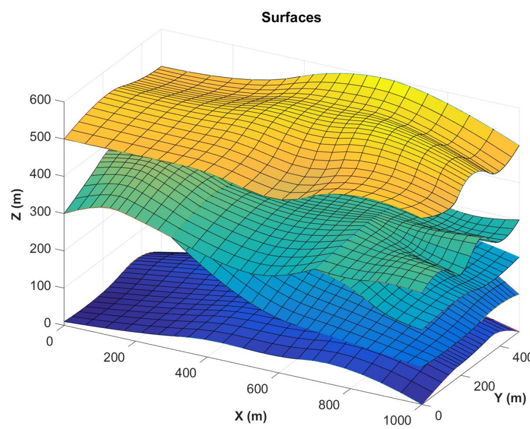

Figure 5: Bilinearly blended Coons patches built from NURBS curves. Colours correspond to heights (z-coordinates). This shows the structured logically Cartesian grids on Coons patches.

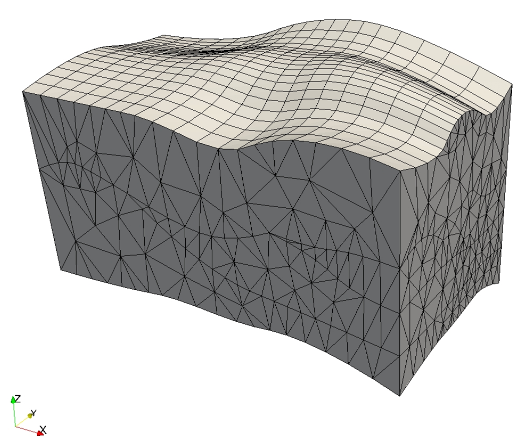

Figure 6: Unstructured hybrid surface mesh in PLC format. Structured grids are built on Coons patches while unstructured grids are on vertical bounding surfaces.

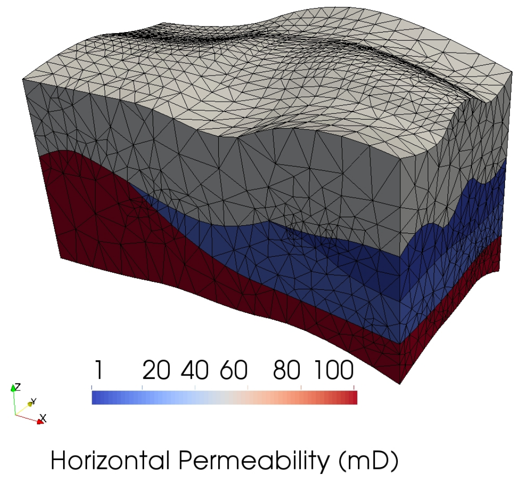

Figure 7: An unstructured tetrahedral volume mesh built from Coons patches. All bounding surfaces and intersection curves are precisely respected. Colours correspond to horizontal permeability values in regions or volumes bounded by surfaces. Steiner points are added on the boundary by TetGen to improve mesh quality.

5.2. Two-Phase Flow Immiscible Displacement

For validating the volume mesh, two-phase incompressible immiscible displacement is simulated. The governing equations are

$$\begin{aligned} \frac{\partial \phi S_\alpha}{\partial t} &= -\nabla \cdot \vec{u}_\alpha + q_\alpha \ , \quad \alpha = o,\ w && (4)\\ \vec{u}_\alpha &= -\frac{k_{r\alpha}}{\mu_\alpha} K(\nabla p_\alpha - \rho_\alpha g \nabla z) \ , \quad \alpha = o,\ w && (5)\\ S_w + S_o &= 1 \ , && (6)\\ p_c &= p_o - p_w && (7) \end{aligned}$$

where o and w denote oil and water which are the non-wetting and wetting phases, respectively. ϕ is porosity, g is gravitational acceleration, p_c is capillary pressure and K is the absolute permeability tensor. For phase α, p_α is pressure, ρ_α is density, S_α is saturation, $\vec{u}_\alpha$ is velocity, μ_α is dynamic viscosity, $k_{r\alpha}$ is relative permeability and q_α is volumetric source term. Oil pressure p_o and water saturation S_w are primary variables. Brooks-Corey model (Brooks and Corey, 1964) is employed for computing relative permeabilities. The residual oil saturation is set to be zero.

$$k_{rw} = \left(\frac{S_w - S_{iw}}{1 - S_{iw}}\right)^4 , \tag{8}$$

$$k_{ro} = \left(\frac{1 - S_w}{1 - S_{iw}}\right)^2 \left(1 - \left(\frac{S_w - S_{iw}}{1 - S_{iw}}\right)^2\right) , \tag{9}$$

where S_{iw} is the irreducible water saturation. The control volume finite element method (CVFEM) (Forsyth et al., 1990) is implemented. In CVFEM, pressure is defined on nodes and is piecewise linear in elements, while saturation is piecewise constant in control volumes. CVFEM benefits from both the accuracy of finite element method and the inherent mass conservation of finite volume method. Here, we assemble fluxes between neighbouring control volumes and store them using an edge-based data structure (see Appendix B).

The mesh and the horizontal permeability field are visualised in Fig. 7. The vertical/horizontal permeability ratio is 0.1. Homogeneous porosity is 0.2. Fluid viscosity is 1 cP. Four injectors are placed on the corners that penetrate the entire formation. A curved producer is inside the model. Injectors have Dirichlet condition of pressure equal to 100 bar. The producer has Dirichlet condition of pressure equal to 1 bar. All other boundaries have no-flow conditions.

The histograms of aspect ratio and dihedral angle of all tetrahedrons are shown in Fig. 8. The aspect ratio of a tetrahedron is its longest edge length divided by its smallest side height (Si, 2013). It is reported that mesh quality mainly affects convergence rather than accuracy for the finite element method (Pointwise, 2012). Accuracy is mainly affected by the numerical scheme for simulation given a fixed mesh resolution (Knupp, 2007).

First, we demonstrate CVFEM is convergent and stable on the mesh in Fig. 7. The steady-state pressure solution is shown in Fig. 9. The boundary between high and low permeability has a high gradient of pressure. A cross-section is presented in Fig. 10 to visualise the curved producer with pressure 1 bar. It is obvious that the tetrahedral elements adapt to the nodes of the producer. The initial saturation of the model is at $S_{iw} = 0.2$. Water is injected and oil is produced. The pressure field is kept constant during water flooding. Fig. 11 presents the water saturation field after 347 days. Both pressure and saturation solutions are physically meaningful indicating that the mesh quality is sufficient for stable pressure and saturation solutions in

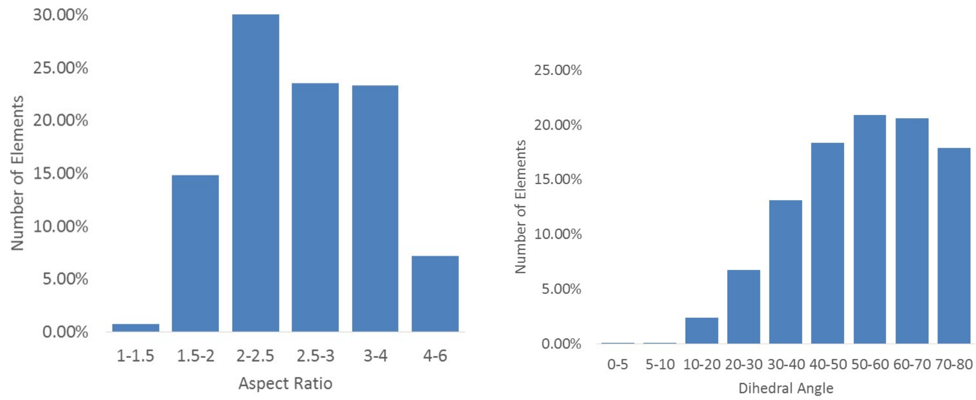

(a) (b)

Figure 8: (a) Histogram of aspect ratio for the surface-based reservoir model. (b) Histogram of dihedral angle of the same mesh.

this example.

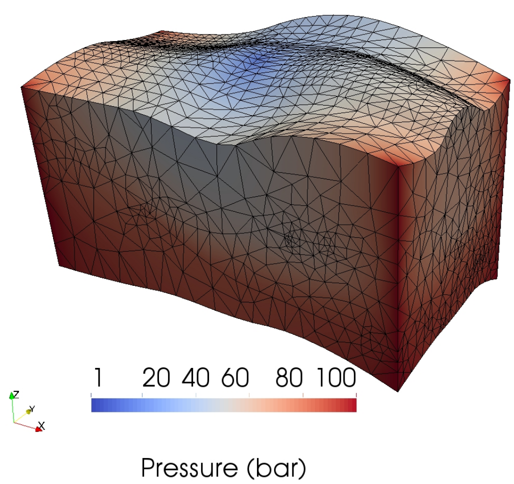

Figure 9: Steady-State pressure field for two-phase immiscible displacement in the surface-based reservoir model. The permeability field is heterogeneous. The boundary between high and low permeability has a high gradient of pressure.

Next, the Buckley-Leverett test case is simulated to validate the accuracy of CVFEM on tetrahedral meshes generated by TetGen against analytical solution. The model dimension is 100 m $\times$ 10 m $\times$ 1 m. The histograms of aspect ratio and dihedral angle of all tetrahedrons in the mesh are exported

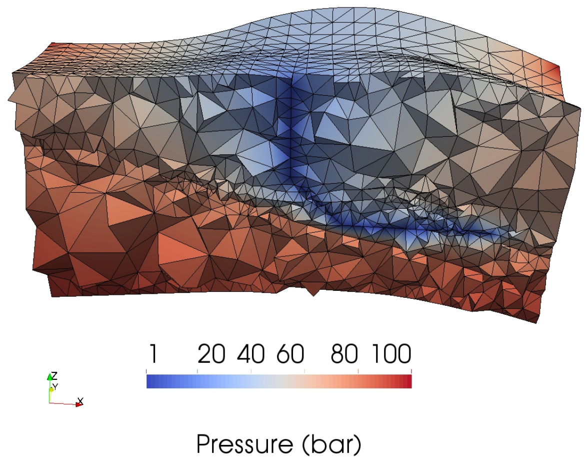

Figure 10: A cross-section to visualise the curved producer with pressure 1 bar. Tetrahedral elements adapt to the well-nodes of the producer.

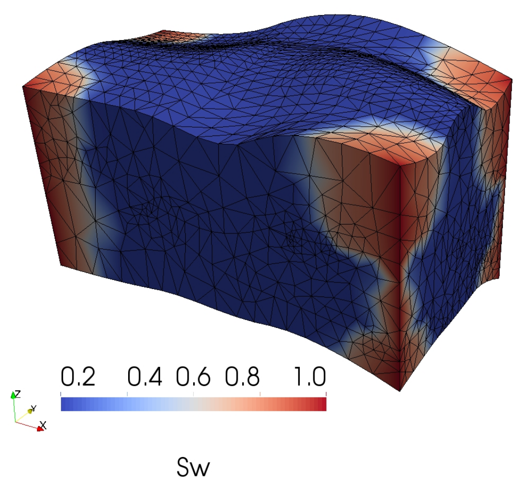

Figure 11: Water saturation field after 347 days for the surface-based reservoir model.

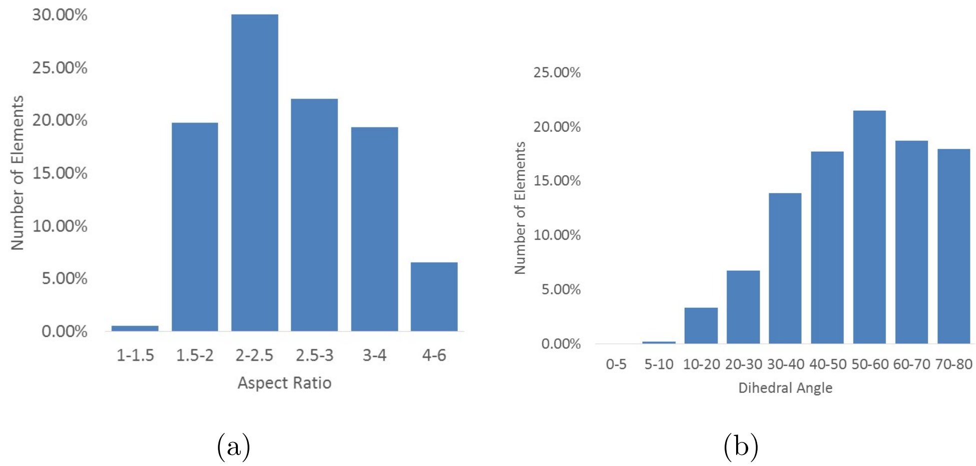

Figure 12: (a) Histogram of aspect ratio for the Buckley-Leverett example. (b) Histogram of dihedral angle of the same mesh.

from TetGen and shown in Fig. 12. The mesh quality of both examples is similar in that the maximum aspect ratio in both cases is below 6 and the maximum dihedral angle in both cases is below 80 degrees, indicating that there is no very bad elements (e.g. an element with > 50 aspect ratio).

The model is fully saturated with oil initially and water is injected from the boundary at $x = 0$ with a constant velocity 9.87×10^{-6} m/s to displace oil. The irreducible water saturation is zero. Homogeneous porosity is 0.2. Both oil and water viscosities are 1 cP. Gravity and capillary pressure are neglected. The 3D water saturation field at $t = 5 \times 10^5$ s and the comparison with analytical result is presented in Fig. 13. The numerical diffusion is due to the single-point upstream weighting for water fractional flow which is first-order accurate. The contact front for the finer mesh is sharper as a consequence of less numerical diffusion.

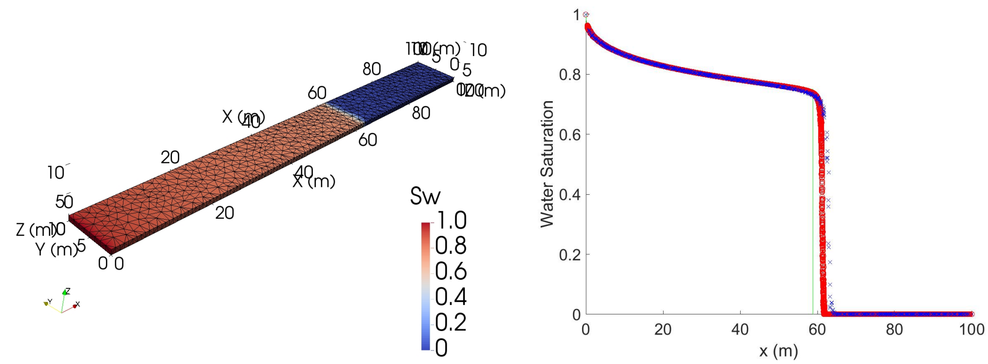

(a) (b)

Figure 13: (a) Buckley-Leverett immiscible displacement on an unstructured tetrahedral mesh. (b) Comparison of numerical and analytical saturation profiles. Blue crosses and red circles are numerical results on course and fine grids, respectively. The green curve is of analytical result.

6. Conclusions

We have presented a workflow for building surface-based reservoir models using NURBS curves, Coons patches and unstructured tetrahedral meshes. NURBS curves are generated to represent the contacts between surfaces and cross-sections. Parametric surfaces are built based on the curves as Coons patches.

Logically Cartesian structured grids are generated on Coons-patches while unstructured triangular meshes are built on vertical bounding surfaces to adapt to internal intersection curves. The hybrid surface mesh of the entire 3D model consisting of triangles and quadrilaterals is constructed by connecting all meshes on individual surfaces.

The surface mesh is stored in PLC format and TetGen is called to build unstructured tetrahedral meshes. The surfaces bounding geological regions are accurately respected by tetrahedral elements. Further constraints can be applied for high-quality mesh generation. Well configurations in terms of location and geometry are particularly flexible, facilitated by local mesh adaptation.

Control volumes are built based on tetrahedral elements to facilitate CVFEM discretisation. An edge-based data structure is used to store the vector area and flux between two neighbouring control volumes. The mesh quality and the accuracy of applying CVFEM on unstructured meshes generated by our workflow have been validated by comparing to the analytical solution of the Buckley-Leverett example.

In our workflow, all libraries for curve, surface and mesh generation are open-source. The benefits are that first, they are free-of-charge for non-commercial uses; second, we have access to the source codes for deeper understanding and better control while commercial software packages may not be fit-for-purpose; third, Triangle and TetGen can be compiled and linked internally without input or output files such that the workflow becomes more efficient; finally, the libraries can be incorporated in software development under proper licenses.

If the bottom-hole pressure (BHP) is of interest, a well model could be applied to couple BHP and well-nodes' pressure (Peaceman, 1978). Fractures will be considered in our future study. The embedded fracture modelling (EDFM) method (Moinfar et al., 2014) will be adopted to avoid the computational complexity involved in adapting the volume mesh to fractures of complex geometry.

Acknowledgements

This paper is from an interesting discussion between authors about using open-source libraries for modelling, meshing and simulation. Our codes are open-source and can be downloaded from the linked Mendeley dataset or by emailing zzhang6666@gmail.com. NURBS Toolbox can be downloaded from https://uk.mathworks.com/ matlabcentral/fileexchange/ 26390-nurbs-toolbox-by-d-m-spink. Triangle can be downloaded from https://www.cs.cmu.edu/ quake/triangle.html. TetGen can be downloaded from http://wias-berlin.de/ software/tetgen/. All these codes should be used together to implement the workflow presented in this paper.

Bibliography

Abdel-Malek, K., Yeh, H.-J., 1996. Determining intersection curves between surfaces of two solids. Computer-Aided Design 28 (6-7), 539–549.

Akkurt, S., Sahin, M., 2017. An efficient edge based data structure implementation for a vertex based finite volume method. In: 23rd AIAA Computational Fluid Dynamics Conference. p. 3292.

Al Qubeissi, M., 2013. Development of a conjugate heat transfer solver. LAP LAMBERT Academic Publishing.

Bentley, M., 2016. Modelling for comfort? Petroleum Geoscience 22 (1), 3–10.

Bentley, M., Ringrose, P., 2017. Future directions in reservoir modelling: new tools and fit-for-purpose workflows. In: Geological Society, London, Petroleum Geology Conference series. Vol. 8. Geological Society of London, pp. PGC8–40.

Borouchaki, H., Laug, P., George, P.-L., 2000. Parametric surface meshing using a combined advancing-front generalized delaunay approach. International Journal for Numerical Methods in Engineering 49 (1-2), 233–259.

Brooks, R., Corey, T., 1964. Hydraulic properties of porous media. Hydrology Papers, Colorado State University.

Cavero, J., Orellana, N. H., Yemez, I., Singh, V., Izaguirre, E., 2016. Importance of conceptual geological models in 3d reservoir modelling. first break 34 (7), 39–49.

Chew, L. P., 1993. Guaranteed-quality mesh generation for curved surfaces. In: Proceedings of the ninth annual symposium on Computational geometry. ACM, pp. 274–280.

Colombera, L., Yan, N., McCormick-Cox, T., Mountney, N. P., 2018. Seismic-driven geocellular modeling of fluvial meander-belt reservoirs using a rule-based method. Marine and Petroleum Geology 93, 553–569.

De Berg, M., Van Kreveld, M., Overmars, M., Schwarzkopf, O. C., 2000. Computational geometry. In: Computational geometry. Springer, pp. 1–17.

Farin, G., Hansford, D., 1999. Discrete coons patches. Computer Aided Geometric Design 16 (7), 691–700.

Farrashkhalvat, M., Miles, J., 2003. Basic Structured Grid Generation: With an introduction to unstructured grid generation. Elsevier.

Forsyth, P. A., et al., 1990. A control-volume, finite-element method for local mesh refinement in thermal reservoir simulation. SPE Reservoir Engineering 5 (04), 561–566.

Guibas, L., Stolfi, J., 1985. Primitives for the manipulation of general subdivisions and the computation of voronoi. ACM transactions on graphics (TOG) 4 (2), 74–123.

Knupp, P., 2007. Remarks on mesh quality. Tech. rep., Sandia National Laboratories (SNL-NM), Albuquerque, NM (United States).

Kumar, A., Camilleri, D., Brewer, M., et al., 2016. Comparative analysis of dual continuum and discrete fracture simulation approaches to model fluid flow in naturally fractured, low-permeability reservoirs. In: SPE Low Perm Symposium. Society of Petroleum Engineers.

Lee, J., 2010. Introduction to topological manifolds. Vol. 940. Springer Science & Business Media.

Lewis, R. W., Nithiarasu, P., Seetharamu, K. N., 2004. Fundamentals of the finite element method for heat and fluid flow. John Wiley & Sons.

Löhner, R., 2008. Applied computational fluid dynamics techniques: an introduction based on finite element methods. John Wiley & Sons.

Lyra, P., Lima, R., Guimarães, C., de Carvalho, D., 2004. An edge-based unstructured finite volume procedure for the numerical analysis of heat conduction applications. Journal of the Brazilian Society of Mechanical Sciences and Engineering 26 (2), 160–169.

Miller, G. L., Talmor, D., Teng, S.-H., Walkington, N., Wang, H., 1996. Control volume meshes using sphere packing: Generation, refinement and coarsening. Fifth International Meshing Roundtable, 47–61.

Milliotte, C., Matthäi, S., 2014. From seismic interpretation to reservoir model: an integrated study accounting for the structural complexity of the vienna basin using an unstructured reservoir grid. First Break 32 (5), 95–101.

Moinfar, A., Varavei, A., Sepehrnoori, K., Johns, R. T., et al., 2014. Development of an efficient embedded discrete fracture model for 3d compositional reservoir simulation in fractured reservoirs. SPE Journal 19 (02), 289–303.

Novakovic, D., White, C. D., Corbeanu, R. M., Hammon Iii, W. S., Bhattacharya, J. P., McMechan, G. A., 2002. Hydraulic effects of shales in fluvial-deltaic deposits: Ground-penetrating radar, outcrop observations, geostatistics, and three-dimensional flow modeling for the ferron sandstone, utah. Mathematical Geology 34 (7), 857–893.

Peaceman, D. W., 1978. Interpretation of well-block pressures in numerical reservoir simulation. SPE Journal 18 (03), 183–194.

Pellerin, J., Botella, A., Bonneau, F., Mazuyer, A., Chauvin, B., Lévy, B., Caumon, G., 2017. Ringmesh: A programming library for developing mesh-based geomodeling applications. Computers & Geosciences 104, 93–100.

Piegl, L., Tiller, W., 2012. The NURBS book. Springer Science & Business Media.

Pointwise, 2012. Accuracy, convergence and mesh quality. Tech. rep., The Connector, Pointwise.

Rogers, D. F., 2000. An introduction to NURBS: with historical perspective. Elsevier.

Ruiu, J., Caumon, G., Viseur, S., 2016. Modeling channel forms and related sedimentary objects using a boundary representation based on non-uniform rational b-splines. Mathematical Geosciences 48 (3), 259–284.

Schreiner, J., Scheidegger, C. E., Fleishman, S., Silva, C. T., 2006. Direct (re) meshing for efficient surface processing. Computer graphics forum 25 (3), 527–536.

Shewchuk, J. R., 1996. Triangle: Engineering a 2d quality mesh generator and delaunay triangulator. In: Applied computational geometry towards geometric engineering. Springer, pp. 203–222.

Shewchuk, J. R., 2002. Delaunay refinement algorithms for triangular mesh generation. Computational geometry 22 (1-3), 21–74.

Shewchuk, J. R., 2005. Tetgen user's manual. University of California at Berkeley.

Si, H., 2013. Tetgen user's manual. WIAS Technical Report No. 13.

Si, H., 2015. Tetgen, a delaunay-based quality tetrahedral mesh generator. ACM Transactions on Mathematical Software (TOMS) 41 (2), 11.

Spink, D., 2010. Nurbs toolbox. https://uk.mathworks.com/matlabcentral/fileexchange/26390-nurbs-toolbox-by-d-m-spink.

Sun, Z., Chew, J. W., Hills, N. J., Volkov, K. N., Barnes, C. J., 2010. Efficient finite element analysis/computational fluid dynamics thermal coupling for engineering applications. Journal of turbomachinery 132 (3), 031016.

Tu, J., Yeoh, G.-H., Liu, C., 2018. Computational fluid dynamics: a practical approach. Butterworth-Heinemann.

Wang, Y., Ma, G., Ren, F., Li, T., 2017. A constrained delaunay discretization method for adaptively meshing highly discontinuous geological media. Computers & Geosciences 109, 134–148.

Welsh, M., Mainland, G., 2004. Programming sensor networks using abstract regions. In: NSDI. Vol. 4. pp. 3–3.

Yin, Z., Ayzenberg, M., MacBeth, C., Feng, T., Chassagne, R., 2015. Enhancement of dynamic reservoir interpretation by correlating multiple 4d seismic monitors to well behavior. Interpretation 3 (2), SP35–SP52.

Zehner, B., Börner, J. H., Görz, I., Spitzer, K., 2015. Workflows for generating tetrahedral meshes for finite element simulations on complex geological structures. Computers & Geosciences 79, 105–117.

Zhang, Z., 2015. Unstructured mesh methods for stratified turbulent flows. Ph.D. thesis, Loughborough University.

Zhao, Y., Zhang, B., 2000. A high-order characteristics upwind fv method for incompressible flow and heat transfer simulation on unstructured grids. Computer methods in applied mechanics and engineering 190 (5), 733–756.

Zhong, D.-H., Li, M.-C., Song, L.-G., Wang, G., 2006. Enhanced nurbs modeling and visualization for large 3d geoengineering applications: an example from the jinping first-level hydropower engineering project, china. Computers & Geosciences 32 (9), 1270–1282.

Zienkiewicz, O., Taylor, R., Zhu, J., 2013. The Finite Element Method: Its Basis and Fundamentals. Elsevier, pp. 151–209.

Appendix A. Unstructured Triangular Mesh Generation on A Single 3D Curved Surface

Since Triangle meshes 2D surfaces, we obtain the corresponding 2D coordinates of points on 3D surfaces, generate 2D meshes and then map them into 3D. This is regarded as an indirect approach for meshing 3D surfaces (Borouchaki et al., 2000; Schreiner et al., 2006). The (u, v) coordinates in the parametrisation of Coons patches in NURBS toolbox could be used as 2D coordinates. However, the range of u and v is $[0, 1]$ which does not contain information of the dimension nor aspect ratio (longest side divided by shortest side) of 3D surfaces. In consequence, a high-quality triangulation in 2D might become skewed and low-quality after being mapped into 3D. To solve the problem, distance coordinates in 2D are defined. For a 3D Coons patch, a logically Cartesian $M \times N$ grid discretising the surface is built to facilitate the computation of distance coordinates. Let $P_{m,n}$ be a node in the structured grid where m and n are along u and v directions, respectively. $1 \le m \le M$ and $1 \le n \le N$. The distance coordinates of $P_{m,n}$ are defined and computed as

$$du_{m,n} = \sum_{i=2}^{m} |\overrightarrow{P_{i-1,n}P_{i,n}}|,\ dv_{m,n} = \sum_{j=2}^{n} |\overrightarrow{P_{m,j-1}P_{m,j}}|\ , \tag{A.1}$$

that can help preserve the dimension of 3D surfaces. For an arbitrary node with parametric coordinates (u, v) on a surface, its 3D coordinates can be obtained as $f(u, v)$ in NURBS Toolbox using the *nrbeval* function. However, we cannot obtain directly parametric nor distance coordinates for an arbitrary node with 3D coordinates; we cannot obtain directly 3D coordinates from distance coordinates. For this, a structured triangular connectivity is established by splitting each quadrilateral cell in the $M \times N$ structured grid into two triangles for mapping between coordinate systems. Vertices of these triangles have known parametric, distance and 3D coordinates. Without loss of generality, mapping from distance to 3D coordinates is illustrated. Let Q be a node with distance coordinates (du_Q, dv_Q) and assume Q lies on a triangle with vertices $i = 1, 2$ and 3 in the structured grid, the 3D coordinates of Q are approximated by the vertices of the triangle as

$$x_Q = \sum_{i=1}^{3} x_i\phi_i,\ y_Q = \sum_{i=1}^{3} y_i\phi_i,\ z_Q = \sum_{i=1}^{3} z_i\phi_i \tag{A.2}$$

where ϕ_i denotes the linear shape function for vertex i. Coordinates of i is (x_i, y_i, z_i). The values of ϕ_i are evaluated using distance coordinates of node Q and the three vertices of the triangle as (Lewis et al., 2004; Zienkiewicz et al., 2013)

$$\phi_1 = \frac{\begin{vmatrix} du_Q & dv_Q & 1 \\ du_2 & dv_2 & 1 \\ du_3 & dv_3 & 1 \end{vmatrix}}{2\begin{vmatrix} du_1 & dv_1 & 1 \\ du_2 & dv_2 & 1 \\ du_3 & dv_3 & 1 \end{vmatrix}}, \ \phi_2 = \frac{\begin{vmatrix} du_1 & dv_1 & 1 \\ du_Q & dv_Q & 1 \\ du_3 & dv_3 & 1 \end{vmatrix}}{2\begin{vmatrix} du_1 & dv_1 & 1 \\ du_2 & dv_2 & 1 \\ du_3 & dv_3 & 1 \end{vmatrix}}, \ \phi_3 = \frac{\begin{vmatrix} du_1 & dv_1 & 1 \\ du_2 & dv_2 & 1 \\ du_Q & dv_Q & 1 \end{vmatrix}}{2\begin{vmatrix} du_1 & dv_1 & 1 \\ du_2 & dv_2 & 1 \\ du_3 & dv_3 & 1 \end{vmatrix}}. \quad \text{(A.3)}$$

Fig. A.14 shows a 3D surface generated as a bilinearly blended Coons patch from four bounding curves. The structured grid is 61×21 for visualisation. Fig. A.15a shows constrained Delaunay mesh generation in the parametric space. The triangulation mapped into 3D is shown in Fig. A.15b where triangles are stretched and of low-quality. Fig. A.16a shows constrained Delaunay mesh generation using distance coordinates instead. Fig. A.16b presents the corresponding mesh in 3D where it can be observed qualitatively that the quality of triangular elements are better than that in Fig. A.15b.

To compare mesh quality quantitatively, the histograms of aspect ratio are presented in Fig. A.17. The aspect ratio of a triangle is defined to be its circumradius over twice its inradius. Assuming the edge lengths are a, b and c, the aspect ratio is equal to $abc/8(s-a)(s-b)(s-c)$ where $s = 0.5(a+b+c)$ (Farrashkhalvat and Miles, 2003). Fig. A.17 shows that the mesh quality in Fig. A.16b using distance coordinates is higher than that in Fig. A.15b using parametric coordinates.

Appendix B. Building Edge-Based Data Structure

A matrix *edgev* is defined to identify local ordering of points for elemental edges (Löhner, 2008)

$$edgev(1:6, 1:2) = \begin{bmatrix} 1 & 2 \\ 2 & 3 \\ 3 & 1 \\ 1 & 4 \\ 2 & 4 \\ 3 & 4 \end{bmatrix} \quad \text{(B.1)}$$

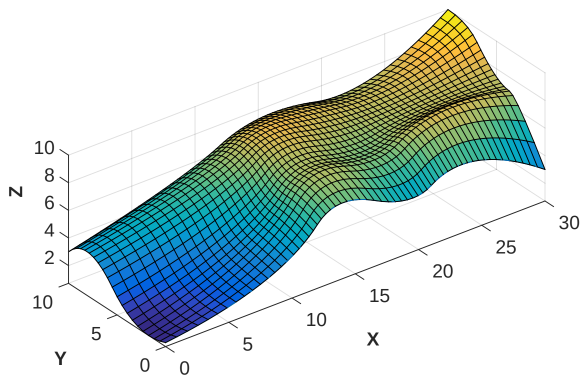

Figure A.14: A 3D surface generated as a bilinearly blended Coons patch from the four bounding curves. Colours reflect heights (z-coordinates).

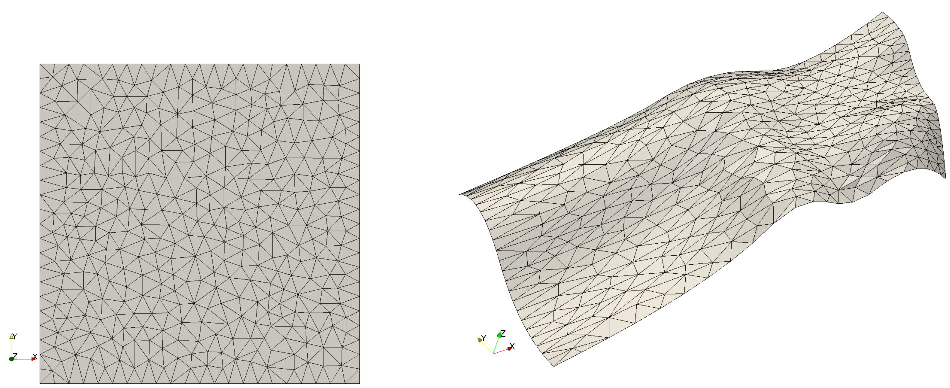

(a) (b)

Figure A.15: Constrained Delaunay triangular mesh generation in the parametric space (a) and the corresponding surface mesh in 3D (b).

For a tetrahedral element, two triangular faces share an edge. The local ordering of faces of elemental edges are stored in $edgef$

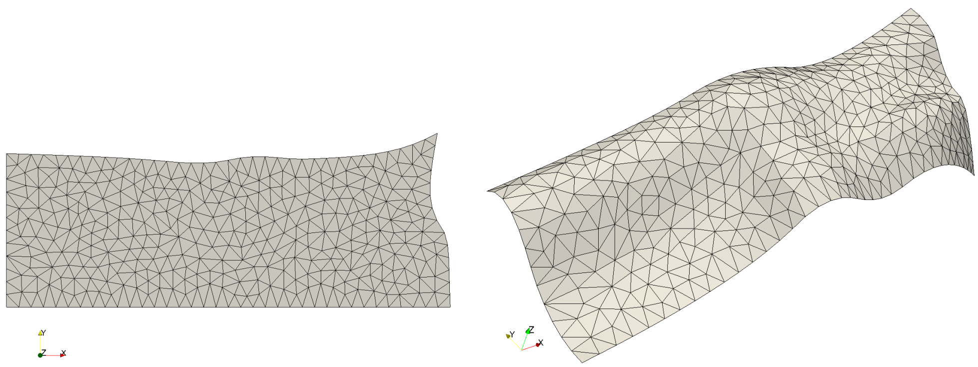

(a) (b)

Figure A.16: Triangular mesh generation of the same quality as in Fig. A.15a using distance coordinates in 2D (a) and the corresponding surface mesh in 3D (b). The quality of the surface mesh in 3D is better than in Fig. A.15b

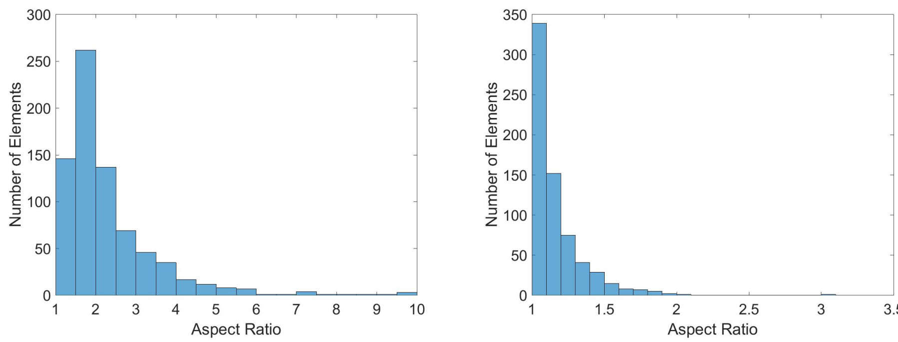

(a) (b)

Figure A.17: (a) Histogram of aspect ratio for 3D surface meshes in Fig. A.15b. Around 54% of triangles have aspect ratio less than 2. (b) Histogram of aspect ratio for that in Fig. A.16b. Almost all triangles have aspect ratio less than 2.

$$edgef(1:6,1:2) = \begin{bmatrix} 4 & 3 \\ 4 & 1 \\ 2 & 4 \\ 3 & 2 \\ 1 & 3 \\ 2 & 1 \end{bmatrix} \tag{B.2}$$

For node-centred finite volume method, vector areas of the shared faces between control volumes around the two endnodes of each edge are assembled and stored on the edge. For control volume finite element method, the fluxes through the shared faces are assembled and stored on the edge. The algorithm based on edges-from-points for computational efficiency. The pseudocodes are presented here.

1. //loop over all elements
2. FOR $iele = 1 \sim nelem$
3.   //obtain the centroid of element $iele$
4.   POINT $point2 = elelist(iele).center$
5.   //loop over all local edges of element $iele$
6.   FOR $i = 1 \sim 6$
7.   //obtain the IDs of two endpoints of a local edge
8. $n1 = elelist(iele).vertex(edgev(i, 1))$
9. $n2 = elelist(iele).vertex(edgev(i, 2))$
10. $i1 = min(n1, n2)$
11. $i2 = max(n1, n2)$
12.   //loop over all edges from the first endpoint
13.   FOR $j = 1 \sim pointlist(i1).edgeout.size$
14.   //obtain the ID of an edge
15. $ied = pointlist(i1).edgeout(j)$
16.   //match the second endpoint
17.   IF $edgelist(ied).vertex(2) == i2$
18.   //the ID of the local edge is found
19. $iedge = ied$
20.   BREAK
21.   ENDIF
22.   ENDFOR
23.   //obtain the midpoint of edge $iedge$
24.   POINT $point1 = edgelist(iedge).center$
25.   //vector from the first to second endpoint
26.   Define vector $\vec{a} = pointlist(i1) \rightarrow pointlist(i2)$
27.   //loop over elemental faces connected to the i'th local edge
28.   FOR $j = 1 \sim 2$
29.   //obtain the centroid of a elemental face

30. POINT $point3 = elelist(iele).face(edgef(i,j)).center$
31. //vectors on a shared boundary face for control volumes
32. Define vector $\vec{b} = point2 \rightarrow point1$
33. Define vector $\vec{c} = point2 \rightarrow point3$
34. //normal vector of a shared face
35. Define vector $\vec{n} = \vec{b} \times \vec{c} / |\vec{b} \times \vec{c}|$
36. $sign = 1$
37. IF $\vec{a} \cdot \vec{n} < 0$
38. $sign = -1$
39. ENDIF
40. //area of shared face
41. $area = 0.5|\vec{b} \times \vec{c}|$
42. //vector area of the face
43. $\vec{S} = \vec{n} \cdot sign \cdot area$
44. //assemble vector areas for edge $iedge$
45. $edgelist(iedge).\vec{S} = edgelist(iedge).\vec{S} + \vec{S}$
46. //flux through the face
47. $flux = elelist(iele).\vec{u} \cdot \vec{n} \cdot sign \cdot area$
48. //assemble fluxes for edge $iedge$
49. $edgelist(iedge).flux = edgelist(iedge).flux + flux$
50. ENDFOR
51. ENDFOR
52. ENDFOR